Lipid nanocapsules for intracellular delivery of microRNA: A first step towards intervertebral disc degeneration therapy

Brian Le Moal, Élise Lepeltier, Dominique Rouleau, Catherine Levisage, Jean-Pierre Benoit, Catherine Passirani, Jérôme Guicheux, Marion Fusellier, Johann Clouet

Lipid nanocapsules for intracellular delivery of microRNA: a first step towards intervertebral disc degeneration therapy

Brian Le Moal[1], Élise Lepeltier[2*], Dominique Rouleau[1,3], Catherine Le Visage[1], Jean-Pierre Benoit[2], Catherine Passirani[2], Jérôme Guicheux[1,4], Marion Fusellier[1,3], Johann Clouet[1,5]

1 *Nantes Université, Oniris, CHU Nantes, INSERM, Regenerative Medicine and Skeleton, RMeS, UMR 1229, F-44000 Nantes, France*
2 *MINT, UNIV Angers, INSERM 1066, CNRS 6021, Angers, France*
3 *Department of Diagnostic Imaging, CRIP, ONIRIS, College of Veterinary Medicine, Food Science and Engineering, Nantes, F-44307, France*
4 *Nantes Université, CHU Nantes, PHU4, F-44000 Nantes, France*
5 *Nantes Université, CHU Nantes, Service Pharmacie, F-44000 Nantes, France*

*Corresponding author:

Dr. Elise Lepeltier, elise.lepeltier@univ-angers.fr, MINT, UNIV Angers, INSERM 1066, CNRS 6021, Angers, France

ABSTRACT

Approximately 40% of cases of lower back pain are caused by disc degeneration disease (DDD). It is well established that microRNA (miR) dysregulation is a key player in various diseases, and its impact on DDD has recently been highlighted. RNAi (miR in particular) is increasingly being considered as a novel therapeutic tool. However, free miR is degraded rapidly *in vivo*, and its protection is thus a prerequisite. Nanoparticular platforms, such as lipid nanocapsules (LNC), could be specifically adapted for miR delivery, allowing the transfer and release of miR in the cell cytoplasm. The objective of the current study was to formulate and characterize miR-loaded LNC to establish their *in vitro* potential (cell internalization, bioactivity) as well as to determine the safety and feasibility of *in situ* intervertebral disc (IVD) injection of miR LNC in a healthy sheep model. Using a miR library, miR-155 was clearly identified as being involved in the DDD process and was selected for further assessment. miR-155-loaded LNC (miR-155 LNC) were successfully formulated using a phase inversion process, with the addition of lipoplexes in the cooling step. Following purification, miR-155 LNC were fully characterized, and the optimized formulation had an average diameter of 75 nm, a polydispersity index below 0.1, and a positive zeta potential. By fluorescence spectroscopy, an encapsulation efficiency (EE) of 75.6% and a drug loading (DL) of 0.6% were obtained, corresponding to a sufficient amount of miR per mL of LNC to potentially have a biological effect. The sustained release of miR-155 from LNC was demonstrated compared with free miR-155: only 22% was released after 2 h and 58% after 24 h. miR-155 protection against endonuclease degradation by LNC was confirmed by gel electrophoresis, *a sine qua non* condition for it to be administered *in vivo*. Cell viability assays were performed on human adipose stromal cells (hASCs) and ovine *Nucleus pulposus* cells (oNP), and a cytotoxicity of less than 30% was obtained at the considered concentrations. Additionally, miR-155 LNC cell internalization was demonstrated by flow cytometry and confocal imaging. Moreover, downregulation of total ERK1/2 in hASCs and oNP cells, after miR-155 LNC treatment, was demonstrated by Western blot and quantitative reverse-transcription PCR (qRT-PCR), thus confirming maintenance of its bioactivity after formulation and internalization. Finally, the feasibility and safety of miR-155 LNC *in situ* injection (compared to control groups: blank LNC and sham condition) was demonstrated in healthy sheep by imaging (MRI and T2wsi measurement) and histology (Boos' scoring) analysis. T2wsi was measured, and no significant difference was observed three months after the injection between the different conditions. No histological impact was observed, with no significant difference in Boos' scoring between the different conditions. All these results suggest LNC may be a potent strategy for the encapsulation and delivery of miR (particularly miR-155) and can be considered as a first step towards IVD regenerative medicine.

KEYWORDS

Intervertebral disc degeneration, lipid nanocapsules, nucleic acid delivery, intradiscal delivery

GRAPHICAL ABSTRACT

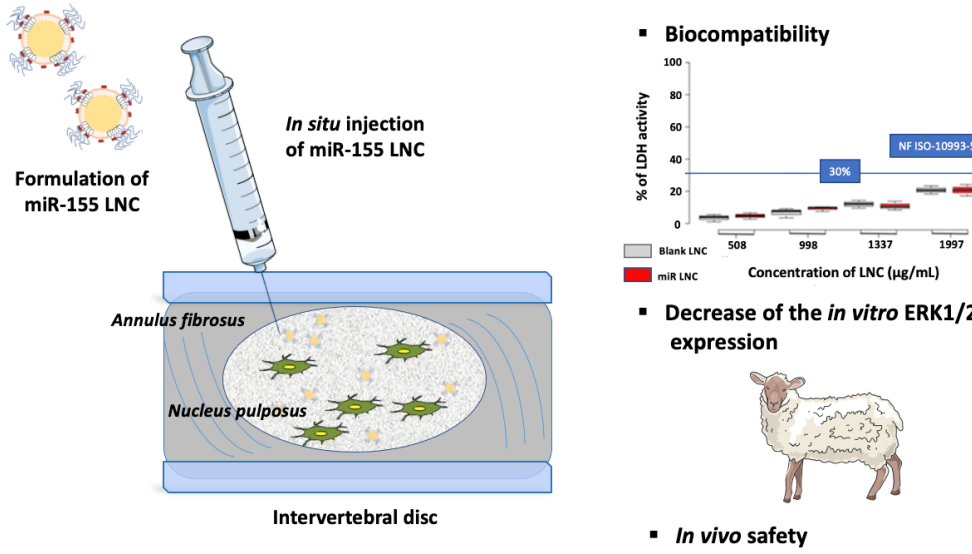

1. INTRODUCTION

Low back pain (LBP), affecting over 80% of adults during their lifetime and resulting in considerable disability and socioeconomic burdens, has been associated with intervertebral disc (IVD) degeneration [1,2]. The IVD, composed of the inner highly hydrated *Nucleus pulposus* (NP), the surrounding *Annulus fibrosus* (AF), and the cartilaginous endplates, is a structure involved in spine flexibility and trunk cinematics. Unfortunately, very early after skeletal maturity, the IVD undergoes a progressive natural aging process, potentially accelerated and amplified by the occurrence of various traumatic, environmental, and genetic factors, corresponding to Disc Degenerative Disease (DDD). DDD is characterized by an increase in catabolic (matrix metalloproteinases (MMP)) and inflammatory factors that drive accelerated extracellular matrix (ECM) degradation, dehydration, and fibrosis, ultimately leading to structural and biomechanical failure [3]. No curative treatment to halt, slow down, or reverse DDD is currently available. Current therapies only address the symptoms (pain relief medication, and surgery). In the past decade, our understanding of DDD has identified new strategies that can not only address the painful symptoms but also the degenerative cascade [4]. Among these novel contemplated therapeutic strategies, cell therapy based on the transplantation of exogenous mesenchymal stromal cells (MSC) has received particular attention and has suggested promising but still inconsistent clinical benefits [5]. In light of the limitations of MSC-based therapies, the development of alternative therapeutics could represent a genuine technological leap forward.

In this context, the recent identification of the role of microRNA (miR) in IVD degeneration allows considering miR as new targets but also as new potential therapeutic agents [6]. Since the discovery of the first miR [7], the field of miR biology has expanded considerably. Insights into the roles of miRs in development and diseases (cancer [8], cardiovascular diseases [9], and inflammatory [10] and autoimmune diseases [11]) have made miR attractive tools and targets for novel therapeutic approaches [12,13]. Of the various miRs expressed in IVD cells and dysregulated in DDD, miR-155, 141, 146a, and 377 have recently been investigated. Their dysregulation in DDD has been proposed as a potential biomarker for early diagnosis of DDD [14,15]. miR-155 in particular has been demonstrated to be a pivotal player in DDD, as a result of its regulatory role in IVD cell apoptosis, ECM synthesis, and inflammation [16–21]. These data make miR-155 one of the most promising candidates as a therapeutic tool to treat DDD.

Despite the huge progress in the fundamental understanding of the role of miRs in the pathogenesis of various diseases, the major challenge to translate their use from the bench to the bedside consists of *in situ* vectorization of these miR to allow their delivery into the target cells where they are expected to exert their therapeutic effects [22]. Direct injection of miRs could be an easy-to-use method, but the effect would typically be short-lived due to the degradation of oligonucleotides by local endonucleases. Improvement of *in vivo* miR delivery has thus been required, and several developments have demonstrated their efficacy [12]. Among these, nanoparticular platforms are considered to be the most likely candidates because they can be a protective carrier for *in situ* vectorization, cell uptake, and intracytoplasmic release of miRs. Notably, lipid nanocapsules (LNC) have been shown to be biocompatible, to have the capacity to protect and release genetic material within the cell, and to have well-controlled physicochemical parameters [23–28]. While the therapeutic efficacy of nanoparticles to systemically deliver miR has been clearly demonstrated in several applications, notably in the treatment of cancer [29,30], data regarding the feasibility of the intradiscal injection (NP transannular injection) of nanoparticles are still missing and remain a prerequisite to support the potential therapeutic applicability of miR in DDD.

In this context, our study aimed to demonstrate the feasibility of miR encapsulation in LNC and to establish the feasibility and the safety of the injection in healthy sheep [31]. To identify

miR-155 as a therapeutic tool and target in the IVD degenerative process, as well as to determine the LNC encapsulation feasibility, miR-155 was used as a model miR in our study.

LNC loaded with miR-155 (miR-155 lNC) were formulated and fully characterized (size, polydispersity index (PDI), zeta potential, efficacy of miR encapsulation, miR release, and protection against endonucleases). Cell internalization of LNC was then demonstrated by confocal imaging and flow cytometry. Two cell types were used to demonstrate cell internalization in a human cell model (hASCs: human adipose stromal cells) and in IVD cells of interest (oNP cells: ovine *Nucleus pulposus* cells). Before undertaking *in vivo* experiments, the metabolic activity and cytotoxicity of LNC on hASCs and oNP cells were evaluated using MTT and LDH assays. Then, the bioactivity of the miR was assessed by Western blot and quantitative reverse-transcription PCR (qRT-PCR) to study the downregulation of extracellular signal-regulated kinases 1/2 (ERK1/2) after miR-155 treatment of hASCs and oNP cells. Finally, the feasibility and safety of miR-155 LNC intradiscal injection (control conditions are blank LNC meaning empty LNC, and sham condition meaning punction of the DIV) was determined in sheep [31] by magnetic resonance imaging (MRI) and histological analyses.

2. MATERIALS AND METHODS

2.1. Materials

Polyoxyl-15-hydroxystearate (Kolliphor® HS15) was purchased from BASF (Ludwigshafen, Germany). Hydrogenated phosphatidylcholine from soybeans (Lipoid S75-3®) was provided by Lipoid GmbH (Ludwigshafen, Germany), and caprylic/capric triglycerides (Labrafac Lipophile WL1349) were supplied by Gattefosse (Saint-Priest, France). DOTAP (1,2-dioleoyl-3-trimethylammonium propane) and DOPE (1,2-dioleoyl-sn-glycero-3-phosphoethanolamine) were purchased from Avanti® Polar Lipids Inc. (Alabaster, Alabama, USA). A Qubit miR Assay Kit®, Alexa Fluor® 488 (Alexa-488), Hoechst 3342, Prolong®, NuPAGE® 3-8% Tris-Acetate gels, and DID were purchased from Thermo Fisher Scientific (Illkirch, France). The miR (miR-155, anti-mi-155, miR control) sense sequences, as well as Alexa Fluor® 488 (Alexa-488) green dye covalently coupled to the miR, were provided by Eurogentec (Liège, Belgium). T75 flasks, DMSO, Tris-EDTA, PBS, BET, DNA loading buffer, chloroform, hyaluronidase H4272 enzyme, trypsin T9935, collagenase C2674, Tris-HCl, potassium chloride, EDTA, EGTA, dithiothreitol, ß-glycerophosphate, Na3VO4, PMSF, NAF, penicillin, streptomycin, Dulbecco's Modified Eagle's Medium (DMEM), and anti-mouse secondary antibodies were purchased from Sigma-Aldrich (St Louis, MO, USA). Anti-ERK1/2 and anti-rabbit secondary antibodies were provided by Cell Signaling (Danvers, MA, USA). NaCl was purchased from ProLabo (Sion, Switzerland). Water was obtained from a Milli-Q® system, Millipore (Darmstadt, Germany). Sephadex® PD10 columns were purchased from Amersham Biosciences Europe (Orsay, France). Dialysis membrane (Spectra/por® float-a-Lyzer®) was purchased from SpectrumLab (Ravensburg, Germany). Ibidi® µ-slide 8-wells were purchased from Ibidi® GmbH (Martinsried, Germany). A NucleoSpin RNAII kit was purchased from Macherey-Nagel (Hoerdt, France). Affinity Script was provided by Agilent Genomics (Santa Clara, CA, USA).

2.2. LNC formulation and characterization

Lipoplex formulation

A cationic lipid DOTAP was chosen to spontaneously self-assemble with the negatively charged miR-155 to form complexes called lipoplexes. A zwitterionic lipid, DOPE, is also added: it is fusogenic and reduces the cytotoxicity of the cationic lipids [32]. Concretely, 52.4 mg cationic lipid DOTAP were dissolved in 2 mL of chloroform and mixed with 57.3 mg DOPE diluted in 2 mL of chloroform, to obtain a final concentration of cationic lipids of 30 mM (1:1 molar ratio of DOTAP/DOPE). After evaporation of the chloroform using a rotary evaporator (Buchi® Rotavapor Evaporator® R-100, Thermo Fisher Scientific), 3 mL of Milli-Q® water was added and left for 1 hour to rehydrate the lipid film. Lipoplexes were then obtained by mixing 750 µg of miR and 378.8 µL of liposomes (from the 3 mL formulation), with a final molar ratio miR/lipids of 0.01, meaning 157 nmol of lipids per µg of miR. Different miR sequences were used: miR-155 sense sequence 5'-GGGCAGUGUUUCAGGCUUATT-3' and non-coding sequence 5'-UUAGCCUGAAACACUGCCCTT-3' miR Ctrl: confidential sequence provided by Eurogentec (Belgium), known to correspond to untargeted human genome Anti-miR-155 (AntagomiR) sense sequence 5'-UGUUAAUGCUAAUAUGUAGGAG-3', and non-coding sequence 5'-CUCCUACAUAUUAGCAUUAACAT-3'

Blank LNC and miR-155/miR ctrl/AntagomiR LNC formulations

The blank LNC were formulated, according to patent US20100233275A1, by mixing 20.5% w/w Labrafac® WL 1349 triglycerides, the lipid core, with 16.9% w/w Kolliphor® HS 15, a hydrophilic surfactant, to allow the phase inversion, with 1.5% w/w Lipoid S75-3®, a hydrophobic surfactant used to provide rigidity for the shell, 1.8% w/w NaCl, and 59.8% w/w Milli-Q® water under magnetic stirring. Three temperature cycles were performed, between 58 °C and 90 °C, leading to the oil in water (o/w) emulsion to water in oil (w/o) emulsion transition, with a phase inversion zone (PIZ) obtained at 78 °C. At this PIZ temperature, rapid cooling and dilution with 3 mL of cold Milli-Q® water resulted in the formation of LNC. To obtain miR loaded LNC (according to patents FR 4185991, 24 Sept 2014 [33]) the Lipoid® was removed from the previous formulation, and 3 mL of lipoplexes were added at the PIZ temperature during

the final temperature cycle. After formulation, miR loaded LNC were purified using a size-exclusion chromatography Sephadex® PD10 column. For 0.5 mL of formulation, a Milli-Q® water elution volume of 20 mL was added. Forty-six fractions were obtained and characterized.

Physicochemical characterization

Size, the polydispersity index (PDI), and the zeta potential of the different fractions were measured by dynamic light scattering and electrophoretic mobility, respectively (Nano series ZS®, Malvern Instruments SA, Worcestershire, United Kingdom), after dilution by a factor of 200 in Milli-Q® water (n = 6).

Encapsulation efficiency and drug loading

The amount of miR-155 obtained in the different fractions after purification using the Sephadex column® was quantified by fluorescence spectroscopy (Fluoromax®, HARIBA, Tokyo, Japan) using a Qubit miR Assay Kit® with the following parameters: excitation wavelength of 545 nm and emission wavelength of 595 nm. To quantify the miR inside the LNC, lysis was performed by a 10-fold dilution in DMSO (n = 3).

The encapsulation efficiency (EE) and the drug loading (DL) were calculated according to the following formulas:

$$EE = \frac{(mass\ of\ miRNA\ measured\ in\ 1\ mL\ of\ LNC) * 100}{initial\ miRNA\ mass\ for\ 1\ mL\ of\ LNC}$$

$$DL(\%\frac{w}{w}) = \frac{mass\ of\ miRNA\ measured\ in\ 1\ mL\ of\ LNC * 100}{mass\ of\ all\ the\ excipients\ in\ 1\ mL\ of\ LNC\ +\ mass\ of\ loaded\ miRNA}$$

miR integrity and protection

The integrity of the miR after LNC formulation was assessed by 4% agarose gel electrophoresis, with the gel containing 1×BET. Different conditions were tested: miR-155 LNC without or with DMSO 1/10 v/v dilution to break the LNC, and miR alone at the same concentration (10 ng/mL). These samples were loaded on the gel after being mixed with loading buffer. Migration was allowed to run for 20 min at 125 V in 1×Tris-EDTA buffer (n = 3). To check the potential protection of the miR by LNC, 0.5 mL human serum (pooled serum, EFS, France) was incubated with 0.5 mL of formulation at 37 °C for 4 h. The same incubation was performed using Milli-Q® water, as a control. Agarose gel electrophoresis of these samples was then performed, as previously described (n = 3).

***In vitro* miR release**

Briefly, 0.5 mL of formulation (blank LNC and miR as controls, and miR-155 LNC) was added to a 100 kDa membrane dialysis bag and then immersed in a beaker containing 35 mL 1×PBS and stirred, at 37 °C. Three batches of 1 mL were then collected at different time points: 30 min, 1, 2, 4, 8, 24, and 48 h. The different samples obtained were then quantified using the Qubit miR assay® (n = 4).

Formulations for the *in vivo* experiments

Regarding *in vivo* experiment specificity, all formulations were validated according to the European Pharmacopeia recommendations (www.edqm.eu). Apyrogenicity, mycoplasma, and bacterial contamination were investigated following protocols adapted from the Nanotechnology Characterization Laboratory (https://ncl.cancer.gov/resources/assay-cascade-protocols).

2.3.Cell experiments

Cell isolation and culture

Human ASCs (hASCs) were obtained from consenting patients undergoing liposuction at the Clinique Breteche (Nantes, France, agreement Agency of Biomedicine PFS08-018). The cells were isolated from the lipoaspirate as previously described [34] and then cultured at 37 °C in a 5% CO_2 incubator with penicillin, streptomycin, and Dulbecco's Modified Eagle's Medium with 1 g/L of L-glucose (DMEM). NP cells were isolated after harvesting of IVDs from sheep (oNP) in collaboration with the National Veterinary School of Nantes (ONIRIS). Briefly, the IVD explants were cut, under sterile conditions, to separate the AF from the NP. The small pieces obtained were rinsed three times in 2% penicillin/streptomycin (P/S) in PBS for 2 minutes. To separate cells from the extracellular matrix, 15–20 mL 0.05% hyaluronidase H4272 in PBS were added and incubated at 37 °C for 15 minutes. After two rinses with PBS, 15–20 mL 0.2% trypsin T9935 in PBS were added and incubated at 37 °C for 30 minutes. After two more rinses with PBS, 15–20 mL collagenase C2674 in complete medium were added and the mixtures were incubated at 37 °C overnight. The recovered suspension was filtered through a 70-µm-pore filter and then centrifuged for 5 minutes at 259 x g. The cells were counted and seeded in T75 flasks at a density of 5.10^3 cells/cm^2.

hASCs and oNP cells (from P0 to P3) were grown at 37 °C and 5% CO_2 in T75 flasks at a starting density of 5.10^3 cells/cm^2 in DMEM supplemented with 10% bovine serum albumin (BSA) and 1% penicillin/streptomycin (P/S) mixture.

Cell internalization (flow cytometry and confocal imaging)

To study the cell internalization, LNC were loaded with a red fluorescent DID dye in the LNC core and an Alexa Fluor® 488 (Alexa-488) green dye was covalently coupled to the miR. During the formulation process, 0.1% w/w DID (0.2 mg) diluted in chloroform was added to the lipid phase.

hASC and oNP cell internalization were first characterized by flow cytometry after incubation with the different formulations (2, 4, 6, and 24 h): (i) LNC labeled with DID (blank LNC); (ii) LNC labeled with DID and loaded with miR control (miR ctrl LNC); (iii) LNC labeled with DID and

loaded with miR-155 labeled with Alexa-488 (miR-155 LNC), and (iv) miR-155 labeled with Alexa-488 (miR-155 alone). The adherent hASCs or oNP cells were trypsinized, resuspended in PBS, and then analyzed using a BD LSRII fluorescence-activated cell sorter (Becton Dickinson, Franklin Lake, NJ, USA). For each sample, 10 000 events were acquired and analyzed using BD FACSDiva® software. The results are expressed on histogram plots as the number of counted cells according to the intensity of the fluorescence in the Alexa-488 and the DID channels (488 and 630 nm, respectively).

For confocal imaging, the hASCs and oNP cells were seeded at 8000 cells/well (0.3 mL) on Ibidi® µ-slide 8-wells. After 24 h, the fluorescent miR-155 LNC were added (79 µg of LNC excipients in 100 µL DMEM) at a concentration corresponding to the optimal concentration of miR for transfection (120 ng miR/100 µL cell medium)[12,35]. After incubation for 8 h, the cells were washed with PBS and then fixed in 4% paraformaldehyde (PFA) (100 µL/well) at 4 °C for 20 min. The PFA was then rinsed using PBS, and nuclear staining was performed by adding 100 µL of 3 µM Hoechst (4',6-diamidino-2-phenylindole) for 10 min in the dark, and then rinsed. All images were obtained using a Leica TCS SP8 AOBS laser scanning confocal microscope (Leica Microsystems, Wetzlar, Germany) equipped with an oil objective lens, HC PL APO CS2 40× / NA 1.10, and controllable hybrid detectors (GaAsP). The images were acquired in the 1024 × 1024 pixels format, a bit depth of 8, and a scan speed of 400 Hz. For the Hoechst, Alexa-488, and DID dyes, excitation was performed using a 405-nm wavelength diode laser (50 mW), a 488-nm wavelength argon-ion laser (40 mW), and a HeNe laser at 633 nm (10 mW), respectively. The detection bandwidth of the emitted light was set between 407 and 480 nm for Hoechst, 488 and 563 nm for Alexa-488, and 635 and 750 nm for DID. Optic sections of the z-series were collected with a width of 1 µm using a "Super Z Galvo Type H internship" and were displayed as maximum z-projections using LAS X software.

Metabolic activity and cytotoxicity (MTT and LDH assays)

The metabolic activity of the hASCs and oNP cells treated by the various LNC formulations was assessed using an MTT assay (M5655, Sigma-Aldrich, St Louis, MO, USA). This assay allows determination of the cell number/cell viability as a function of mitochondrial activity in living cells. The key component is (3-[4,5-dimethylthiazol-2-yl]-2,5-diphenyl tetrazolium bromide), abbreviated as MTT. Mitochondrial dehydrogenases of viable cells cleave the tetrazolium ring, resulting in purple formazan crystals that are insoluble in aqueous solutions. The absorbance of the converted dye is measured at a wavelength of 562 nm. Briefly, the hASCs were seeded in 96-well plates (5000 cells/well) and incubated for 24 h. The medium was then replaced with different concentrations of blank LNC and miR-155 LNC in cell medium (from 508 to 1997 µg/mL LNC) and incubated at 37 °C for 24 h (50 µL of supernatant were removed from each well and used for the LDH test). The absorbance of the samples was recorded at 562 nm using a microplate reader (VIKTOR®, PerkinElmer, Melville, New York, USA). Cytotoxicity was measured by LDH assay (Pierce kit reference 88953, Thermo Fisher Scientific, Saint-Aubin, France). Lactate dehydrogenase (LDH) is a cytosolic enzyme released into the cell culture medium when the plasma membrane is damaged. LDH released in the previously removed 50 µL of supernatant was quantified by a coupled enzymatic reaction in which LDH catalyzes the conversion of lactate to pyruvate via NAD+ reduction to NADH. Oxidation of NADH by diaphorase leads to the reduction of a tetrazolium salt (INT) to a red formazan product that can be measured spectrophotometrically at 490 nm.

In the two assays, the absorbance of cells incubated with DMEM only was considered to represent 100% cell viability (Absve), while the cells treated with 5% Triton X-100 were considered to represent 0% cell viability (Absdc). Metabolic activity (MA) and cytotoxicity were calculated using the following equations:

$$MA\ (\%) = \frac{100 * \left(\mathrm{Abs}_{\mathrm{Sample592nm}} - \mathrm{Abs}_{\mathrm{ve592nm}}\right)}{\left(\mathrm{Abs}_{\mathrm{dc592nm}} - \mathrm{Abs}_{\mathrm{ve592nm}}\right)}$$

$$Cytotox\ (\%) = 100 * \frac{\left(\mathrm{Abs}_{\mathrm{Sample490nm}} - \mathrm{Abs}_{\mathrm{ve490nm}}\right)}{\left(\mathrm{Abs}_{\mathrm{dc490nm}} - \mathrm{Abs}_{\mathrm{ve490nm}}\right)}$$

miR-155 bioactivity

To identify miR bioactivity, gene expression of total extracellular signal-regulated kinases 1/2 (ERK1/2) was assessed using RT-qPCR. Variation of ERK1/2 gene expression was recently identified in NP cells and allowed confirmation of the bioactivity of miR-155 released from LNC [20]. Total RNA was isolated from cells using a NucleoSpin RNAII kit according to the manufacturer's instructions. RNA was reverse transcribed using Affinity Script (Agilent Genomics, Santa Clara, CA, USA). RT-qPCR was performed with a Bio-Rad CFX96 analyzer using a miR-X miR RT-qPCR SYBR Kit® (Takarabio Inc, USA) for miR-155 and SYBR®Select Master Mix (Applied Biosystems, Thermo Fisher Scientific) for ERK1/2. The primer efficiency was determined using a standard curve with a 1:4 v/v dilution, and the specificity of amplification was checked using a melting curve analysis. The expression of target genes was normalized to B2M (beta-2-microglobulin) expression levels, and relative gene expression levels were calculated as previously described [36]. The sequences of the primers used in this study were (forward and reverse):

oNP cells:
ERK1/2: 5'-TGTCAACAAAGTCCGAGTCGCC-3' (forward) and 5'-TGTTCTCGTGTCTGAAGCGCAG-3' (reverse)
B2M: 5'-GGGCTGCTGTCGCTGTCTGG-3' and 5'-TGGCTTTCCATCTCCTGGCGG-3' (reverse)

hASCs:
ERK1/2: 5'-TGGCAAGCACTACCTGGATCAG-3' (forward) and 5'-GCAGAGACTGTAGGTAGTTTCGG-3' (reverse)
B2M: 5'-CCTGGAGGCTATCCAGCGTA-3' (forward) and 5'-GGATGACGTGAGTAAACCTGAATCT-3' (reverse)

miR-155 bioactivity by Western blot
Cells were lysed for 30 min in ice-cold lysis buffer (20 mM Tris-HCl, pH 7.5, 100 mM potassium chloride, 1 mM EDTA, 1 mM EGTA, 1 mM dithiothreitol, 20 mM ß-glycerophosphate, 2 mM Na_3VO_4, 1 mM PMSF, and 1 mM NaF). After centrifugation at 12 000x g for 10 min at 4 °C, the protein extracts (supernatants) were boiled in Laemmli loading buffer prior to SDS-PAGE. Electrophoresis was performed using NuPAGE® 3–8% Tris-acetate gels. Proteins were transferred to a PVDF membrane and blocking was performed with 5% non-fat dry milk/TBST (10 mM Tris, 154 mM NaCl, and 0.15% Tween-20) at room temperature for 1 h. Blots were probed with primary antibodies in 5% non-fat dry milk/TBST at 4 °C overnight, followed by secondary antibodies at room temperature for 1 h. Anti-ERK1/2 was used at a 1:2000 v/v dilution. Monoclonal anti-ß-tubulin clone AC-74 was used at a 1:2000 v/v dilution as a loading control. Anti-rabbit and anti-mouse secondary antibodies were used at 1:2000 and 1:80 000 dilutions, respectively. Signal detection was performed using ECL Western blotting detection reagent with a ChemiDoc Imaging System® (Bio-Rad, Hercules, CA, USA).

2.4.Safety and feasibility of in vivo studies

Ethical aspects and animals
All animal handling and surgical procedures were conducted according to the European Community Guidelines for the Care and Use of Laboratory Animals (DE 86/609/CEE). The Pays de la Loire ethics committee approved the animal study protocol (approval CEEA-PDL APAFIS 26562). Five healthy female sheep (1 to 2 years old; weight, 70 to 90 kg; GAEC HEAS farm, Ligné, France) were used for the study. All animals were followed up for 3 months by daily clinical observation, MRI examination at month (M)0-M1-M3, and histological analysis at M3.

Surgical procedure
Sheep anesthesia was induced by intravenous injection of 2–5 mg/kg of ketamine, 0.2 mg/kg of diazepam, and 1–3 mg/kg of propofol and maintained by inhalation of 1–3% isoflurane. Analgesia was obtained by intravenous injection of 0.5 mg/kg of morphine, then continuous rate infusion of 50-100 µg/kg/min of lidocaine and 0.6-1.2 µg/kg/min of ketamine. The sheep were bedded ventrally [19].

Group organization and formulation safety
Three lumbar intervertebral discs (IVD, n = 25) were randomly assigned to one of the three conditions: *in situ* injection (180 µL) of blank LNC (n = 5), miR-155 LNC (n = 9), or sham condition (control; n = 14). Injection into the NP was performed percutaneously by a transannular approach under fluoroscopic guidance using a 22 G needle, as in the conventional posterolateral procedure [37].

MRI procedure and image analysis
MRI imaging was performed pre- and post-operatively, as well as pre-euthanasia. MRI of the entire lumbar spine was performed using a 1.5 T MRI scanner (Magnetom Essenza®, Siemens Medical Solutions, Erlangen, Germany) with a standard spine coil to obtain T2-weighted images (TE: 86 ms, TR: 3000 ms; slice thickness: 3 mm) and T1-weighted images (TE: 12 ms, TR: 322 ms; slice thickness: 3 mm). The image data were analyzed with Osirix software 3.9 (Osirix Foundation, Geneva, Switzerland). Each IVD was assigned a degenerative score on T2-weighted mid-sagittal images using the Pfirrmann grading [20]. On the mid-sagittal T2-weighted images, an oval region-of-interest (ROI) was drawn around the NP and another on the spinal cord just above the IVD. The T2-weighted signal (T2wsi) was obtained by weighting the NP T2 signal by the spinal cord signal.

Histological analysis
At 3 months after injection, all lumbar IVDs were collected and processed for histological analysis, with fixation in 4% PFA for 5 days, followed by decalcification (Shandon TBD-2® Decalcifier, Thermo Fisher Scientific, Cheshire, UK) for 3 weeks and a post-fixation step in 4% PFA for 24 h. All IVDs were frozen and then cryosectioned (CryoStar NX70®, Thermo Fisher Scientific, Waltham, Massachusetts, USA) at -30 °C in the sagittal orientation into 5 µm sections. Following standard protocols, the sections were stained with hematoxylin-eosin (HE), Masson's trichrome (MT), and Alcian blue (AB). All of the stained sections were observed using a slide scanner (NanoZoomer®, Hamamatsu Photonics, Hamamatsu, Japan) and all of the images were analyzed with NDP.view2® software (Hamamatsu Photonics). The histological sections were analyzed using a Boos' scoring [21] specifically designed to characterize the histomorphology of the IVD and to evaluate the degenerative changes in the extracellular matrix of the NP. Briefly, this modified Boos' scoring was based on the analysis of four criteria: decrease in cell density, granular changes, tear and cleft formation, and mucus degeneration. Some parameters were ranked from 0 to 4 (granular and mucus degeneration) and others were ranked from 0 to 5 (decrease in cell density, and tear and cleft formation) depending on the intensity of the parameters tested (0, lowest; 4 or 5, highest). Three independent investigators, who had expertise in reading histological slides, performed a blind evaluation of histological samples.

2.5.Statistical analysis

The statistical analyses were performed using open-source R software.

For the miR-155 release study, the statistical significance was calculated using the Kruskal–Wallis test. P-values of 0.05 or less were considered to be significant (* $p < 0.05$, ** $p < 0.01$). For the flow cytometry results, the test results were confirmed using the post hoc Bonferroni test.
Pfirrmann grade, T2wsi, and Boos' scoring were assessed for statistically significant differences using the Tukey test, after an analysis of variance test. The significance level was set at 0.05.
All results are presented as means ± SD.

3. RESULTS AND DISCUSSION

3.1. Characterization of blank and loaded LNC

The blank LNC were formulated *via* an inversion phase process. Blank LNC with a diameter of 50.3 ± 2.5 nm, a PDI of 0.03 ± 0.01, and a neutral zeta potential of -1.5 mV ± 1.3 mV were obtained.
The formulation of miR-155 LNC was performed as outlined in the Materials and Methods. The Lipoid® was removed from the previous formulation, and miR-155 lipoplexes were added at the PIZ temperature during the final temperature cycle of the phase inversion process. Purification by size-exclusion chromatography was performed, and 46 fractions were obtained (**Table 1**). The presence of miR-155 in each fraction was quantified by fluorescence spectroscopy. The miR was mainly found in fractions 6 to 13 (96 µg miR for 0.5 mL of formulated LNC). Fractions 1 to 6 corresponded to the liposome-free fraction and fractions 14 to 22 to the diluted LNC formulation. Fractions 23 to 46 corresponded to impurities or aggregates in water [28]. Therefore, only fractions 6 to 13 were used in the rest of the study. The encapsulation efficiency (EE) obtained was 75.6 ± 1.6% and the drug loading (DL) was 0.6 ± 0.01%, corresponding to 590.5 ± 2.5 µg miR-155 per gram of LNC. In comparison, gold–iron oxide nanoparticles loaded with miR were reported to have EE of approximately 84%, with a DL of 0.02% [38]. In another study, the formulation of nanocomposite microparticles to encapsulate miR-146a resulted in an EE of 81% and a DL of 0.4% [39]. Therefore, in our study, the LNC had an EE comparable with other nanoparticle systems, with an improved DL, in accordance with previous studies describing the encapsulation of DNA in LNC [28].

Fractions	Diameter (nm)	PDI	Zeta potential (mV)	Amount of miRNA (ng/mL)
1 to 6	494.0 ± 140.8	0.6 ± 0.20	0.3 ± 0.1	0
6 to 13	75.0 ± 2.4	0.05 ± 0.01	9.6 ± 1.3	96196.7 ± 1789.4
14 to 16	87.5 ± 2.0	0.2 ± 0.11	7.6 ± 1.4	381.0 ± 207.2
17 to 19	104.5 ± 6.9	0.2 ± 0.13	0.7 ± 0.4	192.2 ± 87.1
20 to 22	195.0 ± 58.9	0.4 ± 0.21	ND	64.4 ± 61.6
23 to 25	866.7 ± 243.2	0.9 ± 0.35	ND	6.5 ± 9.4
26 to 28	665.3 ± 361.2	1	ND	18.2 ± 25.6
29 to 31	477.0 ± 144.4	1	ND	41.1 ± 47.8
32 to 34	931.7 ± 313.9	1	ND	12.3 ± 21.2
35 to 37	1052.7 ± 240.2	1	ND	0
38 to 40	941.7 ± 149.6	1	ND	0
41 to 43	1144.7 ± 626.8	1	ND	0
44 to 46	1208.3 ± 330.0	1	ND	0

Table 1: ***Characterization of the different fractions*** obtained after purification using a size-exclusion column: diameter, zeta potential, polydispersity index (PDI), amount of miR per fraction, n = 3 replicates. ND: no reliable value was obtained.

3.2. *miR release from LNC*

The miR-155 release profile from LNC after 48 h was determined in PBS and compared with two controls: miR-155 alone and blank LNC (**Figure 1**). The miR-155 alone rapidly diffused through the dialysis membrane, with 70.4 ± 2.1% of the miR released after 2 h. Interestingly, sustained release was observed for the miR-155 loaded LNC, with only half of the miR-155 released after 24 h, and 80 % after 48 h. The difference between the free miR-155 and the miR-155 LNC was significant after 4 h and 24 h ($p < 0.05$). This experiment confirmed that miR could be slowly released from the LNC when suspended in PBS ([28]). This result has to be considered a first step in the characterization of this nanocarrier, and it is known that this release profile can be modified under real-world conditions, after *in vivo* injection, particularly in the harsh IVD environment, where hypoxia, high pressure, low pH, and low access to nutrients have been identified [40].

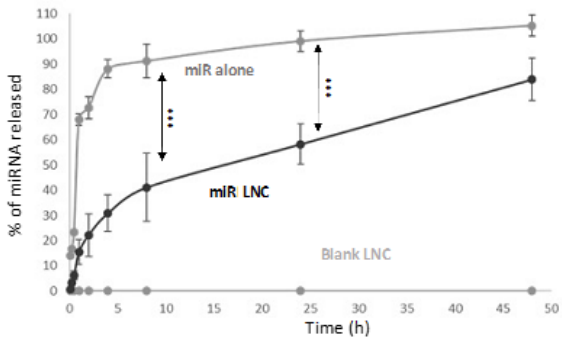

Figure 1: ***Percentage (%) of miR-155 released from LNC in PBS***. miR-155 alone (orange), miR-155 LNC (red), and blank LNC (blue) were investigated. The data are plotted as means ± SD, in triplicate, from three independent experiments; *** $p \leq 0.01$; Kruskal–Wallis test.

3.3. *miR integrity and protection by LNC*

To study the integrity of the miR once formulated, gel electrophoresis was performed after incubation for 4 h in water and in human serum to study potential nuclease protection of the miR-155 by LNC. Different conditions were tested: miR-155 alone, blank LNC, and miR-155 LNC with or without lysis by DMSO (**Figure 2**). DMSO allowed the LNC to break down, leading to miR release [28].

For the free miR-155 condition, after 4 h incubation in water, a band was observed corresponding to the molecular weight of miR-155. In human serum, no miR was detected due to nuclease degradation. For the miR-155 LNC condition, after 4 h incubation in water, a miR-155 band was observed. This result confirms the data shown in **Figure 1,** with a miR-155 release from LNC of 30% after 4 h. No band was observed after incubation in serum, due to enzymatic degradation. Finally, after 4 h of incubation in water and post-treatment by DMSO, a more intense band was observed, corresponding to the total amount of miR released. In human serum, the same band was observed, demonstrating the potential of LNC to protect oligonucleotides from enzymatic degradation. This protection of miR-155 by LNC will be essential against DDD endonucleases [41]. These results are in accordance with previous studies that revealed these potent properties of LNC: drug protection and controlled drug release [28,33,42].

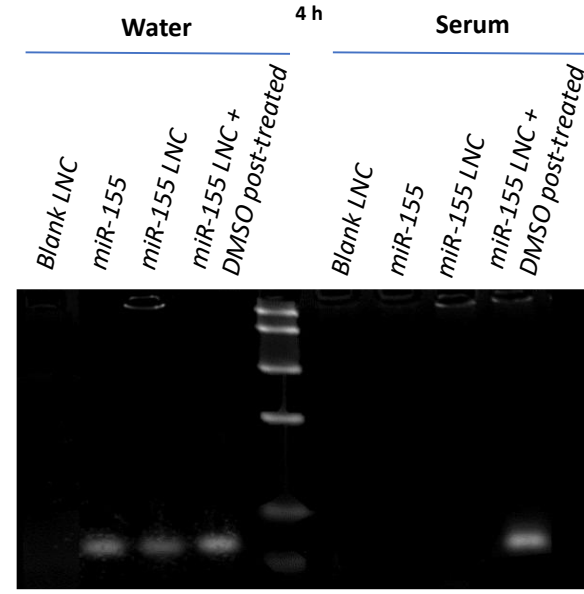

Figure 2: ***Evaluation of miR-155 integrity and protection by LNC, using gel electrophoresis***. LNC, miR-155, and miR-155 LNC were incubated for 4 h in water or human serum. An additional condition (after incubation for 4 h) was assessed using DMSO to lyse the LNC. A miR band, with a molecular weight of 23 bp (15 kDa) was observed by gel electrophoresis. The molecular-weight ladder used was a low-range 1 kb ladder with bands for 1000, 500, 250, 150, 50, and 20 bp. n = 3 (a representative gel is shown).

3.4. *Cell internalization studies*

In order to determine the cell internalization of LNCs, two cell types were used successively: hASCs and oNP cells. hASCs represent a model suitable for verifying, as a first step, possible internalization with the aim of eventual human application. In parallel, oNP cells represent an appropriate model for considering pre-clinical studies in animals. Two methods were used to determine hASC and oNP cell internalization: flow cytometry and confocal imaging. Different conditions were tested after treatment of cells for 2, 4, 6, and 24 h with either: (i) LNC labeled with DID, a red dye (blank LNC); (ii) miR-155 labeled with a green dye Alexa-488 (miR-155 alone), (iii) LNC labeled with DID and loaded with miR control (miR ctrl LNC), and (iv) LNC labeled with DID and loaded with miR-155 and labeled with Alexa-488 (miR-155 LNC), with the same concentration of 998 µg LNC/mL for each condition (**Figure 3**).

As expected, no Alexa-488 fluorescence was observed for the blank LNC or miR ctrl LNC conditions, and no DID fluorescence was observed for the miR alone, in both cell types. A very low degree of internalization of the miR-155 alone was observed, even after 24 h, explained by the miR hydrophilicity, which is known to be involved in communication between cells [43]. However, a significant increase in fluorescence in the Alexa-488 and DID channels was observed over time for the miR-155 LNC condition in both cell types, from 202 ± 35 arbitrary units for cells alone to 155 203 ± 55 604 arbitrary units at 24 h in the DID channel for hASCs and 307 ± 30 arbitrary units to 125 037 ± 100 004 for oNP. Due to the total shift of fluorescence observed, it can be concluded that there was 100% cell internalization. In oNP cells, we observed a broader distribution of the fluorescence in the cells, indicating that some cells internalized less LNC than others. However, the control cells exhibited a total shift of fluorescence, thus confirming that all of the cells had internalized LNC. These results could be explained by ECM synthesized by NP cells in 2D culture before the addition of LNC, which may have impaired the interactions of LNC with oNP cells, thus resulting in limited internalization [44,45].

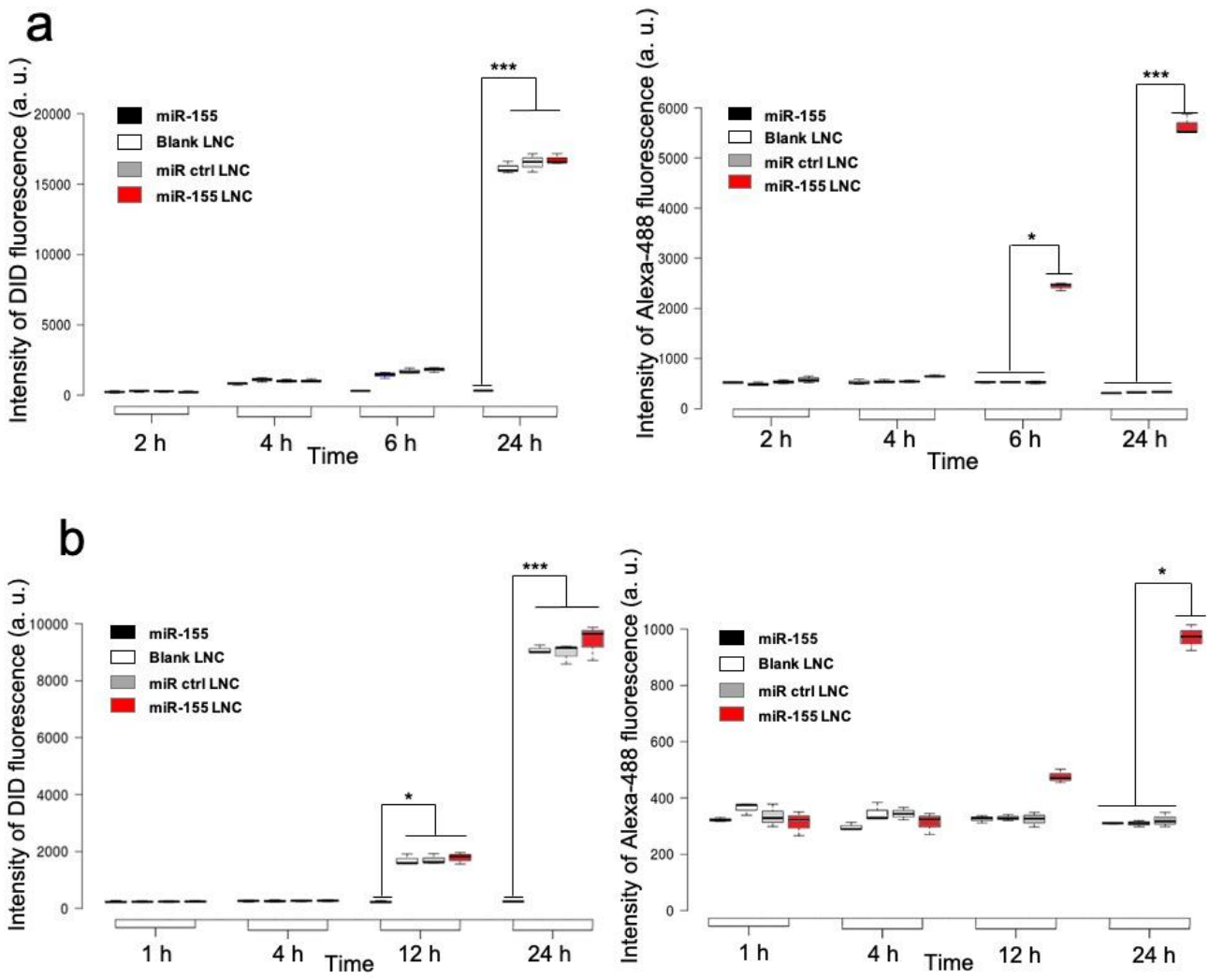

Figure 3: ***Flow cytometry analysis of LNC cell internalization*** in hASCs (a) and oNP cells (b) of blank LNC (LNC-DID) in white, miR-155 (miR-Alexa-488) in black, miR ctrl LNC (LNC-DID with unlabeled miR) in grey, and miR-155 LNC (miR-Alexa-488 loaded LNC-DID) in red, analyzed at different time points (1 h, 2 h, 4 h, 6 h, 12 h, 24 h), with a concentration of 998 µg of LNC/mL of formulation, according to the emission wavelengths used to excite DID (LNC fluorescence) or Alexa-488 (miR fluorescence). n = 3 replicates;median values were analyzed using the Kruskal–Wallis test *$p \leq 0.01$, ***$p \leq 0.005$.

To confirm the FACS data, confocal imaging was performed under the same conditions: blank LNC, miR-155 alone, miR ctrl LNC, and miR-155 LNC (**Figure 4**). The red fluorescence observed was comparable between the blank LNC, the miR-155 LNC, and the miR ctrl LNC. The cell internalization of the LNC was not affected by the miR. No miR-155 green fluorescence was observed when the miR was not protected by the LNC. The green fluorescence from Alexa-488 covalently bound to miR was only observed in the miR-155 LNC condition, after 24 h. Interestingly, there was cytoplasmic localization of miR-155 after internalization in both cell types. The colocalization was confirmed by a Pearson correlation between red and green fluorescence in the three-dimensional z-stack imaging (**Figure S1, A**). The Pearson score obtained was 0.89 for hASCs and 0.79 for oNP, corresponding to a statistically strong colocalization of the green and red fluorescence for both cell types at 24 h. (**Figure S1, B**). Compared to other lipid nanoparticles for delivery of miR, we observed the same internalization speed, with internalization starting at 4h/6h and total internalization at 24 h [46,47]. These results are in accordance with a previous study that used lipid nanocapsules in cancer cells: LNC were fully internalized after 24 h of treatment [28,48]. These results demonstrated that LNC enable miR to be internalized in IVD cells of interest (NP cells) as well as in cells of human origin (hASCs), allowing the potential of our strategy of miR-155 vectorization using LNC to be assessed.

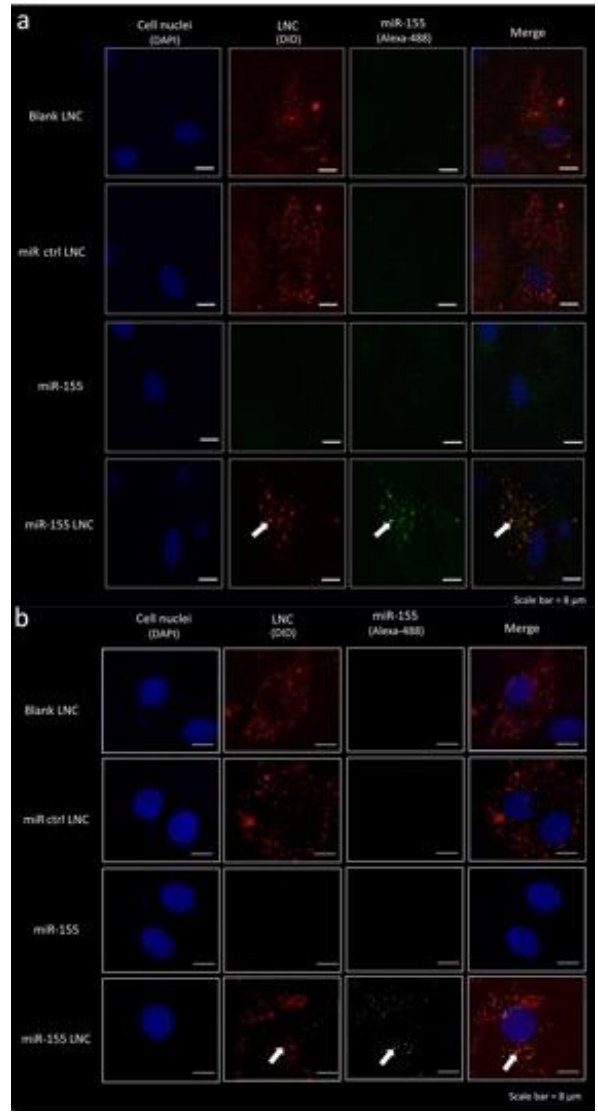

Figure 4: ***Confocal imaging to study cell uptake.*** Cell internalization in hASCs (a) and oNP (b) of miR-155, miR ctrl LNC, blank LNC, miR-155 LNC was assessed after incubation for 24 h with 998 µg LNC/mL. Nuclei, blue; LNC-DID, red; miR, green. Merged conditions, in orange, show a fusion of green (miR) and red (LNC) highlighted by a white arrow. Scale bar = 8 µm. n = 3 replicates (representative images shown).

3.5.Cell viability

After incubation of miR-155-loaded LNC for 24 h, the metabolic activity and the cytocompatibility were studied using MTT and LDH assays, respectively, in oNP cells and hASCs (**Figure 5**). There was a dose-dependent effect on the metabolic activity in both cell lines. In the case of hASCs, the metabolic activity decreased from 84 ± 3% to 60 ± 7% after treatment with 508 µg/mL and 1997 µg/mL in LNC, respectively. In the case of oNP cells, the metabolic activity decreased from 98 ± 9% to 46 ± 4% after treatment with 508 µg/mL and 1337 µg/mL in LNC, respectively. The metabolic activity was even more affected in oNP cells, reaching 46 ± 4% after treatment with 1997 µg/mL in LNC. No significant difference was confirmed by statistical analysis (Kruskal–Wallis test $p > 0.05$, $n = 3$) between blank LNC and miR-155 LNC for both cell models. In parallel to the metabolic activity, no cytotoxicity was confirmed using the LDH assay. In both cell lines, from 508 to 1997 µg/mL of LNC, the *in vitro* cut-off defined in NF-ISO-10993-5 of 70% viability was established, and blank LNC and miR-155 LNC can be considered to be safe for medical purposes [49]. These results thus confirmed that the LNC were not cytotoxic for the studied cells, especially when the LNC concentration was below 998 µg/mL. These data are in accordance with previous reports, where siRNA-loaded LNC were considered to be non-cytotoxic for non-tumor cells, and recently published cytocompatibility results on similar LNC [28,50]. These LNC possess less LDH activity compared with recently developed liposomes encapsulating a 0.2 molar ratio of miR [51]. These results show the cytocompatibility of the miR LNC and they can hence be used for the development of industrialized products for miR delivery. Therefore, compared with liposomes formulated by a process involving organic solvents and known to be unstable in biological fluids, LNC are more promising from an industrial perspective because they are prepared using a solvent-free, soft-energy procedure, and the excipients used are free of genetically modified organism and approved by the US Food and Drug Administration (FDA) [52]. Furthermore, the industrial scale-up of LNC was previously investigated and an easy scalability of production was noted [53]. These features indicate that miR LNC have ample potential as candidates for industrial production and commercialization [54].

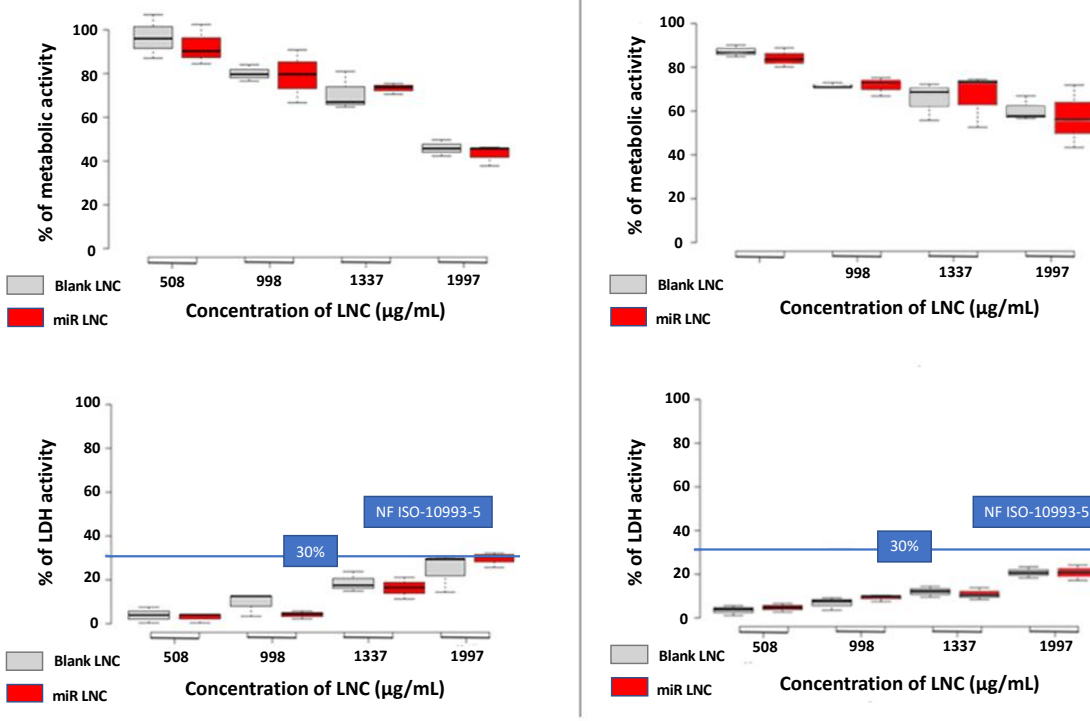

Figure 5: ***Cytocompatibility experiments***. Metabolic activity (MTT assay) and cytotoxicity (LDH test) on hASCs (a) and oNP cells (b) after treatment for 24 h with different concentrations of blank LNC and miR-155-loaded LNC (from 508 to 1997 µg/mL in LNC). The data are plotted as means ± SD; no statistical difference was observed between blank LNC (gray) and miR-155 LNC (red) by the Kruskal–Wallis test. n = 3 replicates

3.6.miR-155 bioactivity

To confirm the bioactivity of miR-155-loaded LNC in hASCs and oNP cells (**Figure 6**), ERK1/2 transcript expression and ERK1/2 protein synthesis were investigated using RT-qPCR and Western blot, respectively. Experiments were performed after 24 h of treatment with miR-155 alone, blank LNC, miR-155 LNC, antagomiR LNC (miR-155-specific targeting), and miR ctrl LNC with the previously used concentration of LNC (998 µg/mL). ERK1/2 is an important protein of the MAPK pathways and is known to be involved in DDD. More specifically, in DDD, ERK1/2 is known to be upregulated, leading to cell death [55]. The results were expressed as transcript expression (2ΔΔCt) relative to the cell control (**Figure 6**). In both cell types, miR-155, blank LNC, and miR ctrl LNC conditions did not significantly modify ERK1/2 expression. Moreover, as expected, miR-155 LNC induced drastic downregulation of ERK1/2 in both cell models. Taken together, these results demonstrated that the miR alone was not sufficiently internalized to have an effect on ERK1/2 protein and gene expression, but when encapsulated in LNC, miR-155 downregulated ERK1/2, as previously described [56]. The results thus proved the efficacy of LNC for delivering miR while maintaining its bioactivity in hASCs and oNP cells.

To complete this study and to elucidate the impact of miR-155 LNC on the ERK/1/2 protein level in hASCs and oNP cells, a Western blot analysis of ERK1/2 total protein synthesis after 24 h of treatment was performed (**Figure 6**). Indeed, ERK1/2 is known to be a specific target of miR-155 in IDD, leading to a reduction of total ERK1/2 protein [56]. When the cells were treated with miR-155 LNC, the protein expression of ERK1/2 was downregulated compared with its expression in the cells alone or treated by blank LNC, miR LNC control, or miR alone. Blank LNC and the miR LNC control had no impact on ERK1/2 protein expression, as expected. miR treatment resulted in the same profile as cells alone, demonstrating that miR alone did not influence the protein expression of ERK1/2, due to its weak internalization. Taken together, these results demonstrated that LNC delivered miR-155 to oNP cells and hASCs while maintaining its biological activity. Here, we demonstrated the biological activity on ERK1/2 as previously published [56]. However, miR-155 is known to target additional genes and proteins in IDD. In IDD, miR-155 is known to target MMP16 and MMP13, which are involved in degradation of the extracellular matrix of the IVD [17], caspase 3, which is involved in Fas-mediated apoptosis leading to cell death of NP cells [18], and C/EBPβ, which leads to reduction of inflammation by downregulation of TNF-alpha and IL-1β [19]. Our results show that the bioactivity of miR-155 is maintained after miR-155 LNC internalization.

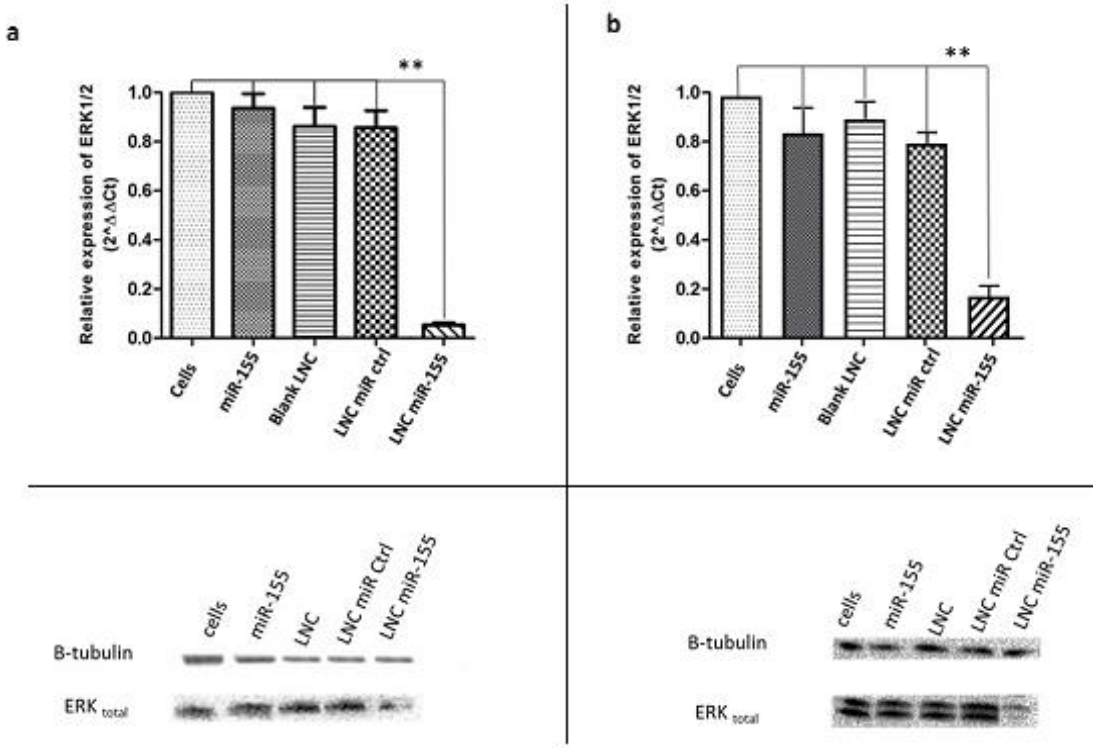

Figure 6: ***Bioactivity of miR-155.*** (a) RT-qPCR (top) and Western blot (bottom) results in hASCs (a) and oNP cells (b) obtained after 24 h of treatment with miR-155, miR ctrl LNC, blank LNC, antagomiR LNC (LNC with antisense miR-155), or miR-155 LNC (998 µg/mL in LNC). The results are presented as means ± SD relative to the cell control. Statistical analysis was performed by comparison of 2ΔΔCt; ** $p < 0.01$, using the Kruskal–Wallis test; representative results are shown.

3.7. *In vivo safety and feasibility of miR-155 LNC injection*

MRI and T2-weighted signal intensity (T2wsi)

In order to evaluate the safety and feasibility of miR-155 LNC injection in sheep IVD, MRI and T2wsi measurements were performed each month for three months after injection, with M0 corresponding to the MRI signal before surgery. No visual difference on MRI was observed during the time of the study or between the different conditions (blank LNC and miR-155 LNC) compared to the control group (**Figure 7a**). T2wsi was then measured to determine the hydration of the IVD (**Figure 7b**). Between M0 and M3, average differences of 1.22 ± 6.8% for the control group, 0.77 ± 8.9% for blank LNC, and 0.48. ± 3.5% for miR-155 LNC were obtained, indicating no significant difference according to the considered month or the studied group. These results indicate there was no significant change in the IVD hydration three months after LNC injection: the hydration being usually correlated with the state of the IVD. In our case, unchanged hydration indicates no negative impact of the LNC injection [35] and confirms the safety and the feasibility of the procedure [36].

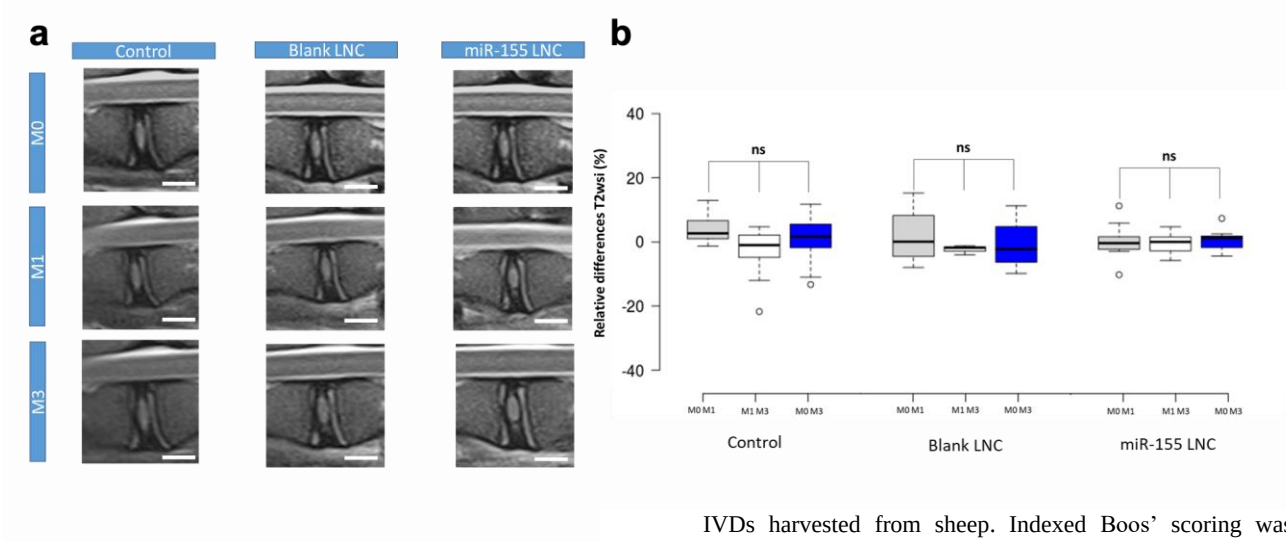

Figure 7: ***MRI images and analysis of lumbar spines in T2wsi*****.** MRI scans with T2wsi signal analysis were performed once a month for 3 months (M0 corresponding to MRI before injection). A total of 25 sheep IVDs were analyzed: 14 for the control, 5 for blank LNC treatment, and 9 for miR-155 LNC. (a) Each month, a magnetic resonance imaging (MRI) scan of the spine was performed. Representative MRI scans are shown. Bar: 3 cm. (b) Representative graph of the relative difference in T2wsi signal, as a percentage, after treatment. At each time point, there was no significant difference between the treated IVDs and the control. Statistical analysis was performed by Kruskal–Wallis test using R software ($p < 0.05$).

Histological staining and Boos' scoring

To complete the MRI and T2wsi measurements, sheep-treated IVDs were collected and cryosectioned, then stained with hematoxylin-eosin (HE), Alcian blue (AB), and Masson's trichrome (MT). HE staining highlights the cellularization of IVDs and the NP/AF collagen content. AB staining shows the good lamella organization of AF and the standard proteoglycan content in AF and NP. Finally, MT staining demonstrates the healthy aspects of endplates. For each condition, hydrated NP were observed, the IVDs maintaining a regular and intact AF organization and lamella alignment. Moreover, proper cellularization was observed for each condition. Finally, to further determine the impact of LNC injection in the IVD, Boos' scoring was performed on the 25 IVDs harvested from sheep. Indexed Boos' scoring was evaluated without the endplate score to focus the scoring on NP and AF aspects, for a maximum score of 23. Boos' scoring was determined by three independent readers well versed in the reading of histological samples. The Boos' scoring obtained was 2.3 for the control group, 4.3 for blank LNC, and 4.1 for miR-155 LNC. There was no significant difference between each group, indicating no significant change between the control and injected groups. This three-month follow-up study of sheep IVDs demonstrated the safety and feasibility of administering miR-155 LNC in IVD.

These *in vivo* results are particularly important before considering the implementation of veterinary (canine patients) or human clinical trials. The choice of the injection surgical route is a topic of active discussion by the scientific community, especially the choice between trans-annular and trans-pedicular surgical routes [37,57,58]. No degeneration process of the control IVDs was observed, thus confirming no negative impact from using the trans-annular surgical route in our study. Coupled with the positive *in vitro* cytotoxicity results, the *in vivo* results support the use of miR-155 LNC in future investigations. In the future, *in vivo* investigation with evaluation of the ERK1/2 protein level and other miR-155 targets by immunohistochemistry of sheep IVDs will have to be performed. The early internalization in NP cells will be also investigated with an *ex vivo* model of IVD culture already

available in our laboratory [59]. *In situ* fluoroscopy will be used to assess this cell internalization.

Moreover, the *in vivo* efficacy of miR-155 or other candidates will be an important issue to define the best target. Indeed, in DDD, numerous miRs are known to be upregulated or downregulated, and the next step of miR therapeutics approach is to combine miRs to impact different metabolic pathways in IVD cells [60]. miR-155 has multiple targets impacting apoptosis, inflammation, and ECM degradation in DDD and it is one of the most represented miR downregulated in DDD [17–19,56,60]. miR-146, which is highly downregulated in DDD, could be also a promising candidate. Combination of miR-155 and miR-146 could be particularly suitable to obtain a synergistic effect. Indeed, miR-146 targets different genes and proteins than miR-155 that are involved in proliferation, the ECM, and inflammation [61–63].

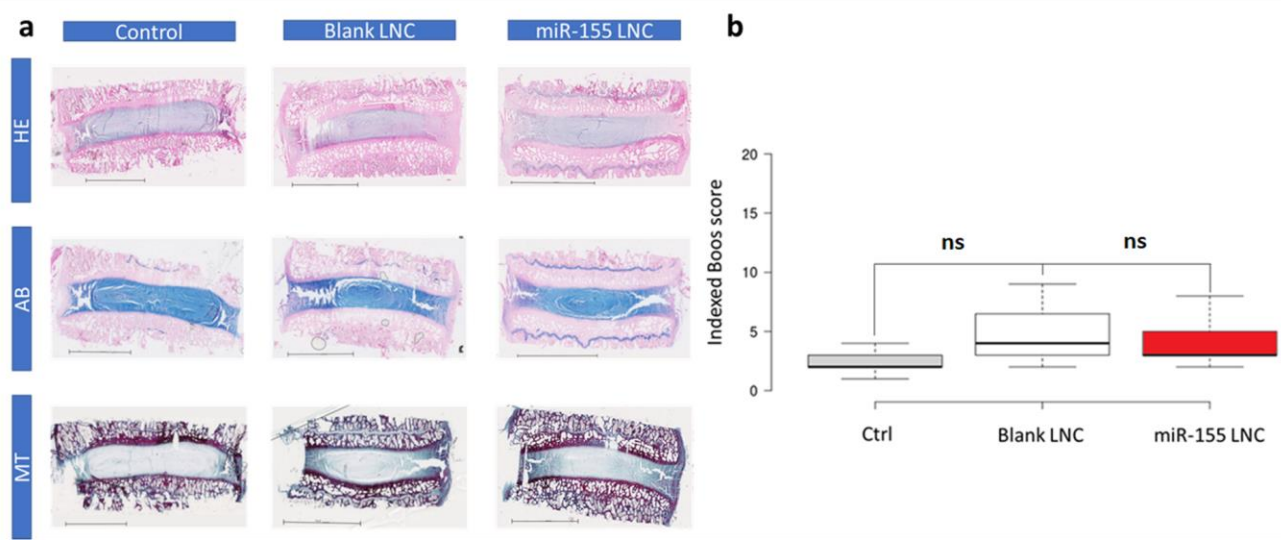

Figure 8*: Histological staining and Boos' scoring of sheep IVDs, 3 months after injection.* (a) Representative sections of endplates 3 months after the injection of blank LNC and miR-155 LNC (70,3 mg/mL). A total of 25 IVDs were collected 3 months after injection with miR-155 LNC or control conditions. Hematoxylin-eosin (HE), Alcian blue (AB), and Masson's trichrome (MT) staining were performed according to the Materials and Method section. No sign of degeneration was observed compared to the control for both blank and miR-155 LNC conditions. (Scale bar = 10 mm), (b) Indexed Boos' scores on NP and AF were determined by three readers on the histological staining. Blank LNC and miR-155 LNC injections had no significant impact on the Boos' scoring. Statistical analysis was performed using R software with the Kruskal-Wallis test and Bonferroni post hoc test ($p < 0.05$).

4. CONCLUSION

In this study, miR-155 LNC were formulated and fully characterized. Characteristics of the LNC system confirmed its potential to vectorize miR, with a promising encapsulation efficiency of 75.6%, a drug loading of 0.6%, and sustained release of miR over 48 h. Moreover, miR protection by LNC from nuclease degradation was demonstrated. The miR-155-LNC internalization was also very satisfactory, showing a high level of cell internalization, allowing almost 100% transfection, with cytoplasmic localization in both ovine and human cell types. Furthermore, miR encapsulation in LNC did not modify its biological activity. The efficacy of LNC in delivering miR was demonstrated while maintaining its bioactivity in both oNP and hASCs. Additional experiments will need to be performed to determine the *in vitro* efficacy of miR-155, or other miR candidates, on cell apoptosis, cell proliferation, extracellular matrix synthesis, and inflammatory processes. Finally, the safety and feasibility of NP injection were confirmed in sheep IVDs. Taken together, these results highlight the high potential of LNC to deliver miR in sheep NP cells, allowing future preclinical efficacy assays, as well as in human cells (hASCs) to be considered, with the aim of future clinical transposition. Additional preclinical experiments in sheep and clinical trials in canine patients will be performed to complete the *in vivo* safety and to determine the *in vivo* efficacy of miR-155, or other miR candidates, to counteract IVD degeneration before their potential use in human clinical trials.

ACKNOWLEDGMENTS

This study was supported by grants from the Institut National de la Santé et de la Recherche Médicale (INSERM), ANR JCJC 2016 (STIMUDISC project ANR-16-CE18-0008), grant "Tremplin clinique vétérinaire" BIOREGATE (Région Pays de la Loire, DISCODOG project), Fondation d'entreprise Grand Ouest BPGO (grant Territoire Recherche 2020, award "Encouragement"). The authors gratefully acknowledge the technical assistance they received from the MINT and RMeS laboratories. The authors gratefully acknowledge Sophie Domingues for editing the paper.

REFERENCES

[1] Global, regional, and national disability-adjusted life-years (DALYs) for 333 diseases and injuries and healthy life expectancy (HALE) for 195 countries and territories, 1990-2016: a systematic analysis for the Global Burden of Disease Study 2016., Lancet (London, England). 390 (2017) 1260–1344. https://doi.org/10.1016/S0140-6736(17)32130-X.

[2] N.N. Knezevic, K.D. Candido, J.W.S. Vlaeyen, J. Van Zundert, S.P. Cohen, Low back pain, Lancet. 398 (2021) 78–92. https://doi.org/10.1016/S0140-6736(21)00733-9.

[3] L. Frapin, J. Clouet, V. Delplace, M. Fusellier, J. Guicheux, C. Le Visage, Lessons learned from intervertebral disc pathophysiology to guide rational design of sequential delivery systems for therapeutic biological factors., Advanced Drug Delivery Reviews. 149–150 (2019) 49–71. https://doi.org/10.1016/j.addr.2019.08.007.

[4] J. Clouet, M. Fusellier, A. Camus, C. Le Visage, J. Guicheux, Intervertebral disc regeneration: From cell therapy to the development of novel bioinspired endogenous repair strategies, Advanced Drug Delivery Reviews. 146 (2019) 306–324. https://doi.org/10.1016/j.addr.2018.04.017.

[5] G. Vadalà, L. Ambrosio, F. Russo, R. Papalia, V. Denaro, Stem Cells and Intervertebral Disc Regeneration Overview-What They Can and Can't Do, Int J Spine Surg. 15 (2021) 40–53. https://doi.org/10.14444/8054.

[6] C. Wang, W.-J. Wang, Y.-G. Yan, Y.-X. Xiang, J. Zhang, Z.-H. Tang, Z.-S. Jiang, MicroRNAs: New players in intervertebral disc degeneration., Clinica Chimica Acta; International Journal of Clinical Chemistry. 450 (2015) 333–341. https://doi.org/10.1016/j.cca.2015.09.011.

[7] R.C. Lee, R.L. Feinbaum, V. Ambros, The C. elegans heterochronic gene lin-4 encodes small RNAs with antisense complementarity to lin-14, Cell. 75 (1993) 843–854. https://doi.org/10.1016/0092-8674(93)90529-Y.

[8] Y. Peng, C.M. Croce, The role of MicroRNAs in human cancer., Signal Transduction and Targeted Therapy. 1 (2016) 15004. https://doi.org/10.1038/sigtrans.2015.4.

[9] S.S. Zhou, J.P. Jin, J.Q. Wang, Z.G. Zhang, J.H. Freedman, Y. Zheng, L. Cai, MiRNAS in cardiovascular diseases: Potential biomarkers, therapeutic targets and challenges re, Acta Pharmacologica Sinica. 39 (2018) 1073–1084. https://doi.org/10.1038/aps.2018.30.

[10] E. Sonkoly, A. Pivarcsi, MicroRNAs in inflammation, International Reviews of Immunology. 28 (2009) 535–561. https://doi.org/10.5001/omj.2012.26.

[11] J.Q. Chen, G. Papp, P. Szodoray, M. Zeher, The role of microRNAs in the pathogenesis of autoimmune diseases, Autoimmunity Reviews. 15 (2016) 1171–1180. https://doi.org/10.1016/j.autrev.2016.09.003.

[12] R. Rupaimoole, F.J. Slack, MicroRNA therapeutics: Towards a new era for the management of cancer and other diseases, Nature Reviews Drug Discovery. 16 (2017) 203–222. https://doi.org/10.1038/nrd.2016.246.

[13] D. Adams, A. Gonzalez-Duarte, W.D. O'Riordan, C.-C. Yang, M. Ueda, A. V. Kristen, I. Tournev, H.H. Schmidt, T. Coelho, J.L. Berk, K.-P. Lin, G. Vita, S. Attarian, V. Planté-Bordeneuve, M.M. Mezei, J.M. Campistol, J. Buades, T.H. Brannagan, B.J. Kim, J. Oh, Y. Parman, Y. Sekijima, P.N. Hawkins, S.D. Solomon, M. Polydefkis, P.J. Dyck, P.J. Gandhi, S. Goyal, J. Chen, A.L. Strahs, S. V. Nochur, M.T. Sweetser, P.P. Garg, A.K. Vaishnaw, J.A. Gollob, O.B. Suhr, Patisiran, an RNAi Therapeutic, for Hereditary Transthyretin Amyloidosis, New England Journal of Medicine. 379 (2018) 11–21. https://doi.org/10.1056/NEJMoa1716153.

[14] M. Ji, H. Jiang, X. Zhang, P. Shi, C. Li, H. Wu, X. Wu, Y. Wang, C. Wang, J. Lu, Preclinical development of a microRNA-based therapy for intervertebral disc degeneration, Nature Communications. 9 (2018) 5051. https://doi.org/10.1038/s41467-018-07360-1.

[15] X. Zhou, L. Chen, S. Grad, M. Alini, H. Pan, D. Yang, W. Zhen, Z. Li, S. Huang, S. Peng, The roles and perspectives of microRNAs as biomarkers for intervertebral disc degeneration, Journal of Tissue Engineering and Regenerative Medicine. 11 (2017) 3481–3487. https://doi.org/10.1002/term.2261.

[16] C. Yang, Z. Shi, J. Hu, R. Wei, G. Yue, D. Zhou, miRNA-155 expression and role in pathogenesis in spinal tuberculosis-induced intervertebral disc destruction., Experimental and Therapeutic Medicine. 17 (2019) 3239–3246. https://doi.org/10.3892/etm.2019.7313.

[17] W.L. Zhang, Y.F. Chen, H.Z. Meng, J.J. Du, G.N. Luan, H.Q. Wang, M.W. Yang, Z.J. Luo, Role of miR-155 in the regulation of MMP-16 expression in intervertebral disc degeneration, Journal of Orthopaedic Research. (2017). https://doi.org/10.1002/jor.23313.

[18] H.Q. Wang, X.D. Yu, Z.H. Liu, X. Cheng, D. Samartzis, L.T. Jia, S.X. Wu, J. Huang, J. Chen, Z.J. Luo, Deregulated miR-155 promotes Fas-mediated apoptosis in human intervertebral disc degeneration by targeting FADD and caspase-3, Journal of Pathology. (2011). https://doi.org/10.1002/path.2931.

[19] J. Zhou, A. Liang, J. Hong, J. Sun, X. Lin, Y. Peng, X. Wang, S. Sun, D. Xiao, K. Xu, W. Ye, MicroRNA-155 suppresses the catabolic effect induced by TNF-α and IL-1β by targeting C/EBPβ in rat nucleus pulposus cells., Connective Tissue Research. 60 (2019) 165–177. https://doi.org/10.1080/03008207.2018.1483356.

[20] D. Ye, L. Dai, Y. Yao, S. Qin, H. Xie, W. Wang, W. Liang, MIR-155 Inhibits Nucleus Pulposus Cells' Degeneration through Targeting ERK 1/2, Disease Markers. 2016 (2016) 6984270. https://doi.org/10.1155/2016/6984270.

[21] S.N. Divi, D.Z. Markova, T. Fang, R. Guzek, M.F. Kurd, J.A. Rihn, A.S. Hilibrand, D.G. Anderson, A.R. Vaccaro, G.D. Schroeder, C.K. Kepler, Circulating miR-155-5p as a Novel Biomarker of Lumbar Degenerative Disc Disease., Spine. 45 (2020) E499–E507. https://doi.org/10.1097/BRS.0000000000003322.

[22] X. Chen, L.S. Mangala, C. Rodriguez-Aguayo, X. Kong, G. Lopez-Berestein, A.K. Sood, RNA interference-based therapy and its delivery systems, Cancer and Metastasis Reviews. 37 (2018) 107–124. https://doi.org/10.1007/s10555-017-9717-6.

[23] B. Heurtault, P. Saulnier, B. Pech, J.-E. Proust, J.-P. Benoit, A novel phase inversion-based process for the preparation of lipid nanocarriers., Pharmaceutical Research. 19 (2002) 875–880. https://doi.org/10.1023/a:1016121319668.

[24] P. Resnier, N. Galopin, Y. Sibiril, A. Clavreul, J. Cayon, A. Briganti, P. Legras, A. Vessières, T. Montier, G. Jaouen, J.-P. Benoit, C. Passirani, Efficient ferrocifen anticancer drug and Bcl-2 gene therapy using lipid nanocapsules on human melanoma xenograft in mouse., Pharmacological Research. 126 (2017) 54–65. https://doi.org/10.1016/j.phrs.2017.01.031.

[25] S. David, T. Montier, N. Carmoy, P. Resnier, A. Clavreul, M. Mével, B. Pitard, J.-P. Benoit, C. Passirani, Treatment efficacy of DNA lipid nanocapsules and DNA multimodular systems after systemic administration in a human glioma model., The Journal of Gene Medicine. 14 (2012) 769–775. https://doi.org/10.1002/jgm.2683.

[26] S. David, C. Passirani, N. Carmoy, M. Morille, M. Mevel, B. Chatin, J.-P. Benoit, T. Montier, B. Pitard, DNA nanocarriers for systemic administration: characterization and in vivo bioimaging in healthy mice., Molecular Therapy. Nucleic Acids. 2 (2013) e64. https://doi.org/10.1038/mtna.2012.56.

[27] P. Resnier, P. LeQuinio, N. Lautram, E. André, C. Gaillard, G. Bastiat, J.-P. Benoit, C. Passirani, Efficient in vitro gene therapy with PEG siRNA lipid nanocapsules for passive targeting strategy in melanoma., Biotechnology Journal. 9 (2014) 1389–1401. https://doi.org/10.1002/biot.201400162.

[28] S. David, P. Resnier, A. Guillot, B. Pitard, J.P. Benoit, C. Passirani, SiRNA LNCs - A novel platform of lipid nanocapsules for systemic siRNA administration, European Journal of Pharmaceutics and Biopharmaceutics. 81 (2012) 448–452. https://doi.org/10.1016/j.ejpb.2012.02.010.

[29] C.P. O'Neill, R.M. Dwyer, Nanoparticle-Based Delivery of Tumor Suppressor microRNA for Cancer Therapy., Cells. 9 (2020). https://doi.org/10.3390/cells9020521.

[30] A. Forterre, H. Komuro, S. Aminova, M. Harada, A Comprehensive Review of Cancer MicroRNA Therapeutic

Delivery Strategies., Cancers. 12 (2020). https://doi.org/10.3390/cancers12071852.
[31] N. Bouhsina, C. Decante, J.B. Hardel, S. Madec, J. Abadie, A. Hamel, C. Le Visage, J. Lesoeur, J. Guicheux, J. Clouet, M. Fusellier, Correlation between magnetic resonance, X-ray imaging alterations and histological changes in an ovine model of age-related disc degeneration, Eur Cell Mater. 41 (2021) 166–178. https://doi.org/10.22203/eCM.v042a13.
[32] L. Ciani, S. Ristori, A. Salvati, L. Calamai, G. Martini, DOTAP/DOPE and DC-Chol/DOPE lipoplexes for gene delivery: zeta potential measurements and electron spin resonance spectra, Biochim Biophys Acta. 1664 (2004) 70–79. https://doi.org/10.1016/j.bbamem.2004.04.003.
[33] P. Resnier, N. Galopin, Y. Sibiril, A. Clavreul, J. Cayon, A. Briganti, P. Legras, A. Vessières, T. Montier, G. Jaouen, J.-P. Benoit, C. Passirani, Efficient ferrocifen anticancer drug and Bcl-2 gene therapy using lipid nanocapsules on human melanoma xenograft in mouse., Pharmacological Research. 126 (2017) 54–65. https://doi.org/10.1016/j.phrs.2017.01.031.
[34] C. Merceron, C. Vinatier, S. Portron, M. Masson, J. Amiaud, L. Guigand, Y. Chérel, P. Weiss, J. Guicheux, Differential effects of hypoxia on osteochondrogenic potential of human adipose-derived stem cells, American Journal of Physiology-Cell Physiology. 298 (2010) C355–C364. https://doi.org/10.1152/ajpcell.00398.2009.
[35] B.B. Shenoda, S. Ramanathan, S.K. Ajit, In Vitro Validation of miRNA-Mediated Gene Expression Linked to Drug Metabolism, Curr Protoc Pharmacol. 79 (2017) 9.26.1-9.26.15. https://doi.org/10.1002/cpph.30.
[36] K.J. Livak, T.D. Schmittgen, Analysis of relative gene expression data using real-time quantitative PCR and the 2(-Delta Delta C(T)) Method., Methods (San Diego, Calif.). 25 (2001) 402–8. https://doi.org/10.1006/meth.2001.1262.
[37] C. Decante, J. Clouet, A. Hamel, L. Le Fournier, O. Gauthier, D. Rouleau, J. Lesoeur, B. Halgand, C. Le Visage, J. Guicheux, M. Fusellier, Collateral effects of targeting the nucleus pulposus via a transpedicular or transannular surgical route: a combined X-ray, MRI, and histological long-term descriptive study in sheep, Eur Spine J. 30 (2021) 585–595. https://doi.org/10.1007/s00586-020-06602-5.
[38] U.K. Sukumar, R.J.C. Bose, M. Malhotra, H.A. Babikir, R. Afjei, E. Robinson, Y. Zeng, E. Chang, F. Habte, R. Sinclair, S.S. Gambhir, T.F. Massoud, R. Paulmurugan, Intranasal delivery of targeted polyfunctional gold–iron oxide nanoparticles loaded with therapeutic microRNAs for combined theranostic multimodality imaging and presensitization of glioblastoma to temozolomide, Biomaterials. 218 (2019) 119342.
[39] A. Mohamed, A.Y. Pekoz, K. Ross, G.A. Hutcheon, I.Y. Saleem, Pulmonary Delivery of Nanocomposite Microparticles (NCMPs) incorporating miR-146a for Treatment of COPD, International Journal of Pharmaceutics. (2019) 118524. https://doi.org/10.1016/j.ijpharm.2019.118524.
[40] N. Henry, J. Clouet, J. Le Bideau, C. Le Visage, J. Guicheux, Innovative strategies for intervertebral disc regenerative medicine: From cell therapies to multiscale delivery systems, Biotechnology Advances. 36 (2018) 281–294. https://doi.org/10.1016/j.biotechadv.2017.11.009.
[41] A.R. Reynolds, S.M. Moghimi, K. Hodivala-Dilke, Nanoparticle-mediated gene delivery to tumour neovasculature, Trends in Molecular Medicine. 9 (2003) 2–4. https://doi.org/10.1016/S1471-4914(02)00004-7.
[42] P. Resnier, T. Montier, V. Mathieu, J.-P. Benoit, C. Passirani, A review of the current status of siRNA nanomedicines in the treatment of cancer, Biomaterials. 34 (2013) 6429–6443. https://doi.org/10.1016/J.BIOMATERIALS.2013.04.060.
[43] R. Bayraktar, K. Van Roosbroeck, G.A. Calin, Cell-to-cell communication: microRNAs as hormones, Molecular Oncology. (2017). https://doi.org/10.1002/1878-0261.12144.
[44] F. Mwale, P. Roughley, J. Antoniou, Distinction between the extracellular matrix of the nucleus pulposus and hyaline cartilage: a requisite for tissue engineering of intervertebral disc, Eur Cell Mater. 8 (2004) 58–63; discussion 63-64. https://doi.org/10.22203/ecm.v008a06.
[45] S.M. Naqvi, C.T. Buckley, Extracellular matrix production by nucleus pulposus and bone marrow stem cells in response to altered oxygen and glucose microenvironments, J Anat. 227 (2015) 757–766. https://doi.org/10.1111/joa.12305.
[46] S.N. Tabatabaei, R.M. Derbali, C. Yang, R. Superstein, P. Hamel, J.L. Chain, P. Hardy, Co-delivery of miR-181a and melphalan by lipid nanoparticles for treatment of seeded retinoblastoma, Journal of Controlled Release. 298 (2019) 177–185. https://doi.org/10.1016/j.jconrel.2019.02.014.
[47] V. Juang, C.-H. Chang, C.-S. Wang, H.-E. Wang, Y.-L. Lo, pH-Responsive PEG-Shedding and Targeting Peptide-Modified Nanoparticles for Dual-Delivery of Irinotecan and microRNA to Enhance Tumor-Specific Therapy, Small. 15 (2019) e1903296. https://doi.org/10.1002/smll.201903296.
[48] S. David, N. Carmoy, P. Resnier, C. Denis, L. Misery, B. Pitard, J.-P. Benoit, C. Passirani, T. Montier, In vivo imaging of DNA lipid nanocapsules after systemic administration in a melanoma mouse model, International Journal of Pharmaceutics. 423 (2012) 108–115. https://doi.org/10.1016/j.ijpharm.2011.06.031.
[49] ISO 10993-5:2009(en), Biological evaluation of medical devices — Part 5: Tests for in vitro cytotoxicity, (n.d.). https://www.iso.org/obp/ui/#iso:std:iso:10993:-5:ed-3:v1:en (accessed October 17, 2021).
[50] M. Szwed, M.L. Torgersen, R.V. Kumari, S.K. Yadava, S. Pust, T.G. Iversen, T. Skotland, J. Giri, K. Sandvig, Biological response and cytotoxicity induced by lipid nanocapsules, J Nanobiotechnology. 18 (2020) 5. https://doi.org/10.1186/s12951-019-0567-y.
[51] S. Sun, H. Zou, L. Li, Q. Liu, N. Ding, L. Zeng, H. Li, S. Mao, CD123/CD33 dual-antibody modified liposomes effectively target acute myeloid leukemia cells and reduce antigen-negative escape, International Journal of Pharmaceutics. 568 (2019) 118518. https://doi.org/10.1016/J.IJPHARM.2019.118518.
[52] J. Hureaux, F. Lagarce, F. Gagnadoux, A. Clavreul, J.-P. Benoit, T. Urban, The adaptation of lipid nanocapsule formulations for blood administration in animals., International Journal of Pharmaceutics. 379 (2009) 266–9. https://doi.org/10.1016/j.ijpharm.2009.05.033.
[53] J. Hureaux, F. Lagarce, F. Gagnadoux, M.C. Rousselet, V. Moal, T. Urban, J.P. Benoit, Toxicological study and efficacy of blank and paclitaxel-loaded lipid nanocapsules after i.v. administration in mice, Pharmaceutical Research. 27 (2010) 421–430. https://doi.org/10.1007/s11095-009-0024-y.
[54] O. Thomas, F. Lagarce, Lipid nanocapsules: A nanocarrier suitable for scale-up process, Journal of Drug Delivery Science and Technology. 23 (2013) 555–559. https://doi.org/10.1016/S1773-2247(13)50084-0.
[55] E. Tsirimonaki, C. Fedonidis, S.G. Pneumaticos, A.A. Tragas, I. Michalopoulos, D. Mangoura, PKCε signalling activates ERK1/2, and regulates aggrecan, ADAMTS5, and miR377 gene expression in human nucleus pulposus cells, PLoS ONE. 8 (2013) e82045. https://doi.org/10.1371/journal.pone.0082045.
[56] D. Ye, L. Dai, Y. Yao, S. Qin, H. Xie, W. Wang, W. Liang, MIR-155 Inhibits Nucleus Pulposus Cells' Degeneration through Targeting ERK 1/2, Disease Markers. 2016 (2016) 1–7. https://doi.org/10.1155/2016/6984270.
[57] L. Le Fournier, M. Fusellier, B. Halgand, J. Lesoeur, O. Gauthier, P. Menei, C. Montero-Menei, J. Guicheux, J. Clouet, The transpedicular surgical approach for the development of intervertebral disc targeting regenerative strategies in an ovine model, Eur Spine J. 26 (2017) 2072–2083. https://doi.org/10.1007/s00586-017-5199-z.
[58] G. Vadalà, F. Russo, G. Pattappa, D. Schiuma, M. Peroglio, L.M. Benneker, S. Grad, M. Alini, V. Denaro, The transpedicular approach as an alternative route for intervertebral disc regeneration, Spine (Phila Pa 1976). 38 (2013) E319-324. https://doi.org/10.1097/BRS.0b013e318285bc4a.

[59] L. Frapin, J. Clouet, C. Chédeville, C. Moraru, E. Samarut, N. Henry, M. André, E. Bord, B. Halgand, J. Lesoeur, M. Fusellier, J. Guicheux, C. Le Visage, Controlled release of biological factors for endogenous progenitor cell migration and intervertebral disc extracellular matrix remodelling, Biomaterials. 253 (2020) 120107. https://doi.org/10.1016/j.biomaterials.2020.120107.

[60] J. Zhu, X. Zhang, W. Gao, H. Hu, X. Wang, D. Hao, lncRNA/circRNA-miRNA-mRNA ceRNA network in lumbar intervertebral disc degeneration., Molecular Medicine Reports. (2019). https://doi.org/10.3892/mmr.2019.10569.

[61] R.-S. Yang, Y.-H. Wang, C. Ding, X.-H. Su, X.-B. Gong, MiR-146 regulates the repair and regeneration of intervertebral nucleus pulposus cells via Notch1 pathway., European Review for Medical and Pharmacological Sciences. 23 (2019) 4591–4598. https://doi.org/10.26355/eurrev_201906_18036.

[62] Y. Xi, T. Jiang, W. Wang, J. Yu, Y. Wang, X. Wu, Y. He, Long non-coding HCG18 promotes intervertebral disc degeneration by sponging miR-146a-5p and regulating TRAF6 expression, Scientific Reports. 7 (2017) 13234–13234. https://doi.org/10.1038/s41598-017-13364-6.

[63] S.-X. Gu, X. Li, J.L. Hamilton, A. Chee, R. Kc, D. Chen, H.S. An, J.-S. Kim, C. Oh, Y.-Z. Ma, A.J. van Wijnen, H.-J. Im, MicroRNA-146a reduces IL-1 dependent inflammatory responses in the intervertebral disc, Gene. 555 (2015) 80–87. https://doi.org/10.1016/j.gene.2014.10.024.